

Photonic Fractional-Order Differentiator Using an SOI Microring Resonator With an MMI Coupler

Hiva Shahoei, *Student Member, IEEE*, Dan-Xia Xu, Jens H. Schmid, and Jianping Yao, *Fellow, IEEE*

Abstract—An optically tunable fractional order temporal differentiator implemented using a silicon-on-insulator microring resonator with a multimode interference (MMI) coupler is proposed and experimentally demonstrated. Through changing the input polarization state, the self coupling coefficient and the loss factor of the designed ring resonator with the MMI coupler are changed. Correspondingly, the coupling regime is changed. Through changing the coupling regime from over-coupled to under-coupled regime, the phase shift in the resonance wavelength is changed from $<\pi$ to $>\pi$. This tunable phase shift is used to implement a tunable fractional order photonic differentiator with an order tunable from <1 to >1 . The proposed fractional order differentiator is demonstrated experimentally. A Gaussian pulse with a bandwidth of 45 GHz is temporally differentiated with a tunable order of 0.37, 0.67, 1, 1.2, and 1.3.

Index Terms—Silicon photonics, SOI microring resonator, optical differentiator.

I. INTRODUCTION

A TEMPORAL differentiator is one of the basic processing blocks that provides temporal differentiation of the complex envelope of an arbitrary input optical pulse. In addition to signal processing purposes [1], an optical temporal differentiator has other potential applications such as pulse shaping [2], [3], pulse coding [4], and optical sensing and control [5]. Different schemes have been presented recently to implement an all-optical temporal differentiator, including cross-gain modulation in a semiconductor optical amplifier (SOA) [6], the use of a long period fiber grating [7], an interferometer [8], a phase shifted fiber Bragg grating [9], or a silicon microring resonator [10]–[12]. In addition to a regular first-order differentiator, a temporal differentiator with a fractional order has also been implemented based on different methods such as asymmetrical phase-shifted fiber Bragg grating (PS-FBG) [13]. One important feature that is not achieved in the previous works is the order tunability. We have recently proposed a continuously tunable fractional order temporal differentiator by using a tilted fiber Bragg grating (TFBG)

written in an Er-Yb co-doped fiber. Due to the strong absorption of the Er-Yb co-doped fiber, when it is optically pumped, the refractive index is changed, which leads to the tuning of the fractional order [14]. The major limitation of the TFBG-based differentiator is the relatively large size and high sensitivity to environmental changes.

In this letter, we propose and demonstrate a tunable fractional order differentiator implemented based on a silicon ring resonator with a multimode interference (MMI) coupler. Since the resonator is fabricated on a silicon chip, the size is small and the stability is significantly improved. The MMI coupler is optimized for the TM (transverse-magnetic) mode, thus by changing the input polarization state, the self-coupling coefficient and the loss factor (α) are changed. Correspondingly, the coupling regime is changed. It can be tuned from the over-coupled regime to the under-coupled regime, which leads to the change of the phase shift at the resonance wavelength from values less than π to values higher than π . This tunable phase shift ($n\pi$) can be used to implement an n th-order all-optical temporal differentiator with the order fully tunable from 0 to 2. The effect of the tunable self-coupling coefficient and the loss factor on the coupling regime and correspondingly on the resonance and the phase shift are studied by simulations. A fractional order temporal differentiator based on a microring resonator is studied theoretically and demonstrated experimentally. A Gaussian pulse with a bandwidth of 45 GHz is temporally differentiated with a tunable differentiation order at 0.37, 0.67, 1, 1.2, and 1.3.

II. PRINCIPLE

An n th-order temporal differentiator provides n th order time derivative of the complex envelope of an input signal $x(t)$, $dx^n(t)/dt^n$. The differentiator can be considered as an optical filter with a frequency response given by

$$H_n(\omega) = [j(\omega - \omega_0)]^n = \begin{cases} e^{jn(\frac{\pi}{2})} |(\omega - \omega_0)|^n & \omega > \omega_0 \\ e^{jn(-\frac{\pi}{2})} |(\omega - \omega_0)|^n & \omega < \omega_0 \end{cases} \quad (1)$$

As can be seen an n th-order temporal differentiator can be implemented using an optical filter that has a magnitude response of $|(\omega - \omega_0)|^n$ and a phase jump of $n\pi$ at ω_0 . An optical filter with a frequency response given by (1) can be implemented using an MMI-coupled SOI ring resonator. In the over-coupling regime, a phase shift of less than π can be achieved while in the under coupling regime, a phase shift of greater than π can be achieved. For a ring resonator with an MMI coupler, its self-coupling coefficient and the loss

Manuscript received April 15, 2013; revised May 28, 2013 and May 31, 2013; accepted May 31, 2013. Date of publication June 4, 2013; date of current version July 9, 2013. This work was supported by the Natural Science and Engineering Research Council of Canada.

H. Shahoei and J. Yao are with the Microwave Photonics Research Laboratory, School of Electrical Engineering and Computer Science, University of Ottawa, Ottawa ON K1N 6N5, Canada (e-mail: jpyao@eecs.uottawa.ca).

D.-X. Xu and J. H. Schmid are with the Institute for Microstructural Sciences, the National Research Council of Canada, Ottawa ON K1A 0R6, Canada.

Color versions of one or more of the figures in this letter are available online at <http://ieeexplore.ieee.org>.

Digital Object Identifier 10.1109/LPT.2013.2266252

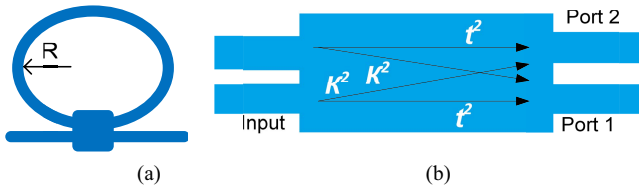


Fig. 1. (a) Microring resonator with an MMI coupler; (b) a close-up view of the MMI coupler.

factor are tunable by changing the polarization. A schematic of an MMI-coupled ring resonator is illustrated in Fig. 1(a). The power splitting ratio to port 1 (t^2) and port 2 (K^2) are governed by $t^2 + K^2 = 1$, as indicated in Fig. 1(b).

Mathematically, the frequency response of an MMI-coupled ring resonator can be expressed as [15], [16],

$$T = \alpha_{MMI} \left[\frac{t - \alpha e^{j\theta}}{1 - \alpha t e^{j\theta}} \right], \quad (2)$$

where $\theta = 2\pi n_{eff}L/\lambda$ is the total round trip phase accumulation, L is the ring cavity length, $\alpha = \alpha_{MMI} \cdot \alpha_{ring}$ is the combined field amplitude loss factor including both ring propagation loss α_{ring} and the coupler loss α_{MMI} , n_{eff} is the waveguide effective index, and λ is the wavelength in vacuum. Thus, the power transmission is given by

$$|T|^2 = \alpha_{MMI}^2 \left[\frac{\alpha^2 - 2\alpha t \cos \theta + t^2}{1 - 2\alpha t \cos \theta + \alpha^2 t^2} \right] \quad (3)$$

To explore the effect of changing the self-coupling coefficient and losses on the coupling regime and consequently on the phase change, three cases are studied by simulations. In the first case, the loss coefficient is constant ($\alpha = 0.77$) and the self-coupling coefficient is changed. The MMI coupler in the SOI microring resonator is optimized for TM mode coupling. For TE input polarization (transverse electric), the self-coupling and the loss coefficient show strong wavelength dependence. For the chosen operating wavelength, the self-coupling coefficient is decreased. By decreasing the coupling coefficient from 0.83 to 0.71, the coupling regime is changed from the over-coupling regime ($t > \alpha$) to the critical coupling regime ($\alpha = t$) and finally the under-coupling regime ($t < \alpha$). As can be seen in Fig. 2(a), the depth and the bandwidth of the resonance is changing during this coupling regime change and consequently the amount of the phase shift is changed from less than π , to π and finally to greater than π , as shown in Fig. 2(b). In the second case, the self-coupling coefficient is constant ($t = 0.83$) and the loss factor is changed. By changing the input polarization from a TM to a TE mode, the total loss factor is increased in the designed ring at the operating wavelength. As can be seen in Fig. 2(d), by changing the loss factor from 0.75 to 0.79, the coupling regime is changed from the over-coupling regime ($t > \alpha$) to the critical coupling regime ($\alpha = t$) and finally to the under-coupling regime ($t < \alpha$). Fig. 2(c) and (d) shows the transmission magnitude and the phase of the ring resonator at different coupling regimes. As can be seen in Fig. 2(d), the phase shift is changed from less than π , to π and to greater than π . Thus, by changing the polarization from a TM to a TE mode

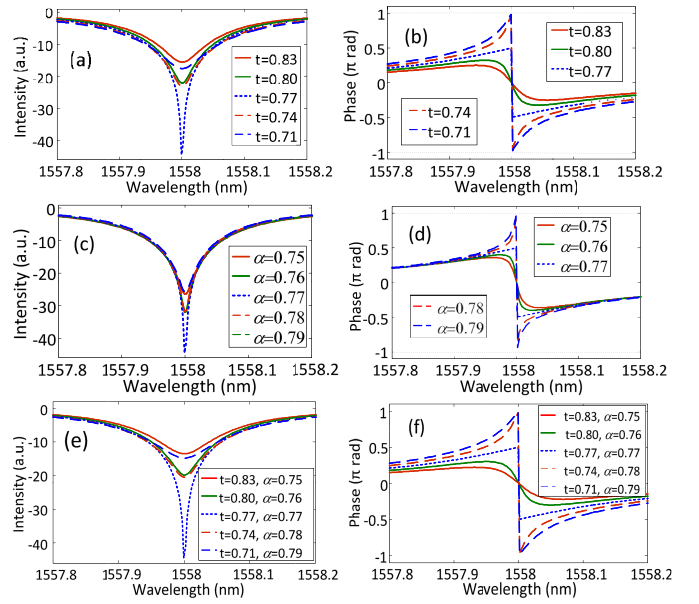


Fig. 2. Simulated transmission magnitude and the corresponding phase for (a, b) $\alpha = 0.77$, and $t = 0.83, 0.8, 0.77, 0.74, 0.71$, (c, d) $t = 0.77$, $\alpha = 0.75, 0.76, 0.77, 0.78, 0.79$, and (e, f) different t , and α .

the coupling regime is tuned from the over-coupling regime to the under-coupling regime and the phase shift is increased from less than π to greater than π . In the third case, both the self-coupling coefficient and the loss factor are changed. By changing the polarization of the input light from a TM to a TE mode, both above cases are applied; the self-coupling coefficient is decreased and the loss factor is increased. Since the effects of these two changes are in the same line, the effect of changing the polarization to the introduced phase shift would be higher. Fig. 2(e) and (f) shows the impact of changing the polarization from a TM to a TE mode on the introduced phase shift. The phase changes of the TE and TM modes are different. If a pulse has a polarization state just in between, then the total phase change is a vector sum of the two phase terms. As can be seen in Fig. 2 a fully tunable phase shift ($n\pi$) is achieved at the center of the resonance, which can be used to implement an n th-fractional order all-optical differentiator with a tunable n between 0 and 2.

An MMI-coupled SOI ring resonator is fabricated on a SOI wafer that has a 260 nm thick silicon layer on a $2\text{-}\mu\text{m}$ thick BOX layer. Waveguides of 450 nm wide are patterned by e-beam lithography and etched in an inductively coupled plasma (ICP) RIE system using C4F8/SF6 chemistry. Inverse tapers down to 150 nm in width are adopted at both the input and output facets to improve the waveguide to fiber coupling efficiency. The perimeter of the ring is $300\ \mu\text{m}$. The cross section of the ring and the bus waveguides is $450\ \text{nm} \times 260\ \text{nm}$. The upper cladding is a layer of SU8 polymer. The MMI coupler has a width and a length of $2\ \mu\text{m} \times 15\ \mu\text{m}$, and the edge separation of the input/output waveguides is $550\ \text{nm}$. Fig. 3(a) shows the measured transmission spectrum of the ring (solid line) with a perimeter of $300\ \mu\text{m}$ at a resonance wavelength of 1558 nm. The measured phase response of the ring around the resonance is shown in Fig. 3(b). The simulated

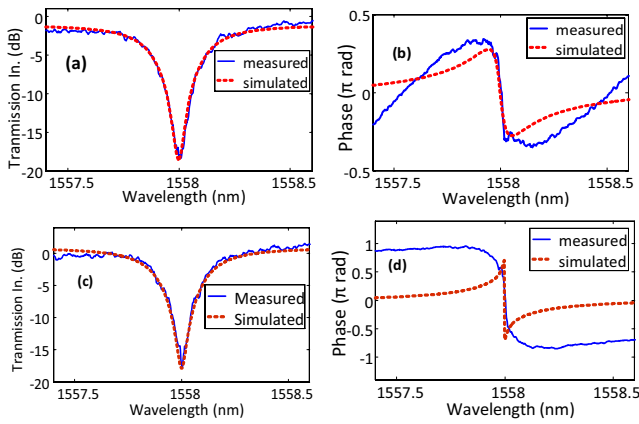


Fig. 3. The magnitude (a, c) and phase response (b, d) of the ring operating in transmission at 1558 nm for two different input polarization states. The coupling regime for the first polarization state is the over-coupled regime and the second polarization state is changed to the under coupled regime. The solid lines show the measured spectrums and the dashed lines show the simulated spectrums.

magnitude and phase responses are also shown as dashed lines for comparison. The parameters of the MMI coupler used in the simulations are $t = 0.804$ and $\alpha = 0.75$. The coupling regime is over coupling and thus the measured phase shift introduced at the center of the resonance is equal to 0.4π (smaller than π), as can be seen in Fig. 3(b), which is very close to the simulated phase shift. Fig. 3(c) and (d) shows the measured (solid line) and simulated (dashed line) magnitude and phase responses of the same ring resonator but for an input light at a different input polarization state. As discussed above, by changing the polarization state of the input light, the resonance shape is changed. The parameters for the MMI coupler used in the simulations are changed to $t = 0.743$ and $\alpha = 0.79$. The coupling regime of the ring is changed to the under-coupling regime, and thus the corresponding phase shift is changed to 1.35π (larger than 1), as can be seen in Fig. 3(d), which is again close to the simulated phase shift. Thanks to the coupling regime change, different phase shift ($n\pi$) can be achieved at the resonance wavelength, by centering an input pulse at this wavelength, an n th-order differentiation of the input pulse can be implemented. It should be noted that for the implementation of a differentiator, the phase response is more important than the magnitude response [14]–[17]. The magnitude response of an ideal temporal differentiator which is given by $|\omega - \omega_0|^n$ may not be exactly satisfied by using the transmission band of the ring resonance, but the phase response plays the key role.

To evaluate the impact of polarization change on the differentiation operation, a Gaussian pulse with a temporal full width at half maximum (FWHM) of 22 ps is used as an input. Differentiated pulse by using the ring in the over-coupling regime with the spectral response shown in Fig. 3(a), corresponding to a differentiator of an order of 0.4, is calculated which is shown as the solid line in Fig. 4(a). A simulated differentiated pulse by an ideal differentiator with an order of 0.4 is also shown as a dotted line. As can be seen the shapes of the differentiated pulses are close, which confirms that the ring resonator is performing as a differentiator with

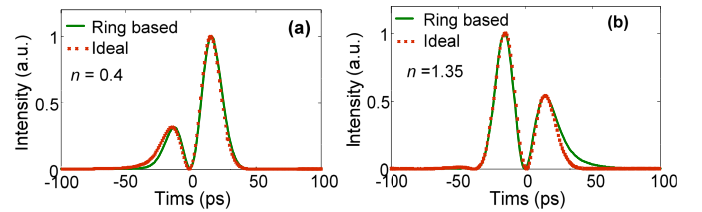


Fig. 4. The simulated differentiated pulse by using the resonances of the ring resonator shown in (a) Fig. 3(a), over-coupled regime, and (b) Fig. 3(b), under-coupled regime. The dotted lines show the simulated differentiated pulses with an ideal differentiator with the orders of (a) 0.4 and (b) 1.35.

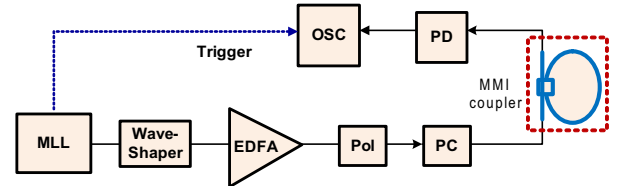


Fig. 5. Experimental setup. MML: mode lock laser. EDFA: Erbium doped fiber amplifier. Pol: Polarizer. PC: polarization controller. PD: photodetector. OSC: oscilloscope.

an order of 0.4. It also confirms that the phase response plays a more important role in the operation. Fig. 4(b) shows the differentiated pulse in the under-coupling regime with the spectral response of the ring shown in Fig. 3(b), corresponding to a differentiator of an order of 1.35. Again a differentiated pulse by an ideal differentiator with the order of 1.35 is shown Fig. 4(b) in dotted line. A good agreement is achieved between the differentiated pulses.

III. EXPERIMENT

An experiment based on the setup shown in Fig. 5 is performed. A short Gaussian pulse with a temporal FWHM of 550 fs, centered at 1558.5 nm is generated by a mode locked laser (MLL). A WaveShaper is used to shape the Gaussian pulse to have a temporal FWHM of 22 ps (corresponding to a spectral width of 45 GHz) centered at 1558 nm. An erbium-doped fiber amplifier (EDFA) connected at the output of the WaveShaper is used to amplify the optical signal. A polarizer (Pol) is used to make the light from the EDFA linearly polarized, and a polarization controller (PC) connected to the Pol is to control and tune the polarization state of the input light to the ring. The light coupled into and out the bus waveguides of the ring is achieved by two tapered fibers. The differentiated signal is detected by a 53-GHz photodetector (PD) and its waveform is observed by a sampling oscilloscope (OSC).

The shaped pulse at the output of the Waveshaper is shown in Fig. 6(a). An ideal Gaussian pulse with the same temporal width (22 ps) is also shown in Fig. 6(a) (dashed line) for comparison. As can be seen experimentally generated input pulse is close to a Gaussian except a slight deviation in the front tail. The polarization state of the input pulse is controlled by tuning the PC. The differentiated pulse is detected by the PD and the waveform is observed by the OSC. A differentiated pulse with a order of $n = 1, 1.2, 1.5, 0.67,$ and 0.37 is

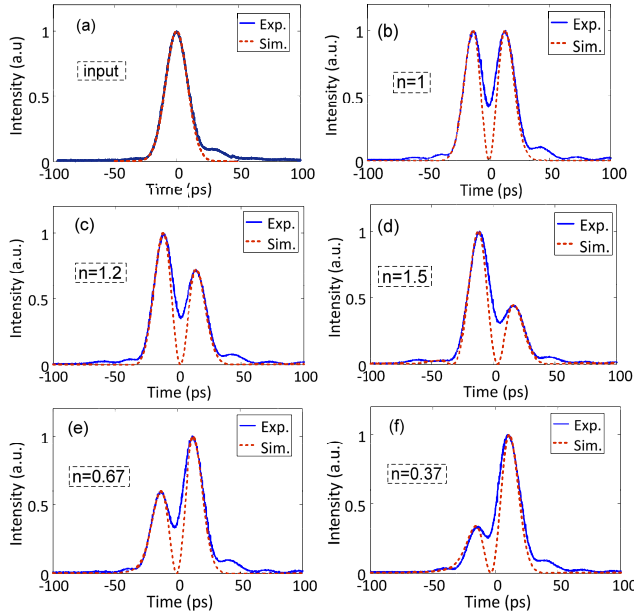


Fig. 6. (a) An input Gaussian pulse with an FWHM of 22 ps, and the differentiated pulses at the different input polarization states corresponding to differentiation orders of (b) $n = 1$, (c) $n = 1.2$, (d) $n = 1.5$, (e) $n = 0.67$, and (f) $n = 0.37$.

generated and shown in Fig. 6(b), (c), (d), (e), and (f). Simulated pulses with an ideal input Gaussian pulse and an ideal differentiator with the same orders are also shown in Fig. 6 (b)-(f), as dashed lines. As can be seen a good agreement is achieved between the experimentally generated pulses and the pulses with an ideal differentiator. The root mean square error (RMSE) in the worst case (Fig. 6 (f)) is equal to 8%. It should be noted that the difference in the notch is caused mainly due to the limited bandwidth of the PD (53 GHz), and the difference in the tail part due to the non-ideal input Gaussian pulse, shown in Fig. 6(a).

IV. CONCLUSION

By changing the polarization state, the round-trip phase accumulation for the TE and TM modes would be different because of different refractive indices. Correspondingly, the resonance wavelength would be shifted. Based on the experiment, for our used ring resonator, however, the resonance wavelength at 1558 nm was almost unchanged when changing the polarization. The largest change was less than 0.01 nm. This would change the differentiation order by 4% which is small and negligible. If the change of the resonance wavelength is large, the optical carrier of the signal to be differentiated should be tuned correspondingly, which may increase the tuning complexity. A simpler solution is to redesign the waveguide geometry to compensate the difference in the round-trip phase accumulation between TE and TM modes [16].

In conclusion, a silicon photonics based continuously tunable n th-order temporal differentiator was proposed and experimentally demonstrated. To the best of our knowledge, this is the first time that a ring-resonator-based temporal differentiator was implemented with a continuously tunable order. The key to achieve the differentiation order tuning was based on the tuning of the input polarization, which led to the change of the coupling regime, resulting in the tuning of the phase shift. It was demonstrated that phase shift could be tuned from 0.3π to 1.7π , corresponding a fractional order from 0.3 to 1.7. The differentiation of a Gaussian pulse with a bandwidth of 45 GHz with different fractional orders was implemented.

REFERENCES

- [1] F. Li, Y. Park, and J. Azaña, "Complete temporal pulse characterization based on phase reconstruction using optical ultrafast differentiation (PROUD)," *Opt. Lett.*, vol. 32, no. 22, pp. 3364–3366, Nov. 2007.
- [2] J. P. Yao, F. Zeng, and Q. Wang, "Photonic generation of ultra-wideband signals," *J. Lightw. Technol.*, vol. 25, no. 11, pp. 3219–3235, Nov. 2007.
- [3] Y. Park, M. Kulishov, R. Slavik, and J. Azaña, "Picosecond and subpicosecond flat-top pulse generation using uniform long-period fiber gratings," *Opt. Express*, vol. 14, no. 26, pp. 12670–12678, Dec. 2006.
- [4] J. A. N. da Silva and M. L. R. de Campos, "Spectrally efficient UWB pulse shaping with application in orthogonal PSM," *IEEE Trans. Commun.*, vol. 55, no. 2, pp. 313–322, Feb. 2007.
- [5] N. Q. Ngo, S. F. Yu, S. C. Tjin, and C. H. Kam, "A new theoretical basis of higher-derivative optical differentiators," *Opt. Commun.*, vol. 230, nos. 1–3, pp. 115–129, Jan. 2004.
- [6] J. Xu, X. Zhang, J. Dong, D. Liu, and D. Huang, "High speed all optical differentiator based on semiconductor optical amplifier and optical filter," *Opt. Lett.*, vol. 32, no. 13, pp. 1872–1874, Jul. 2007.
- [7] R. Slavik, Y. Park, M. Kulishov, R. Morandotti, and J. Azaña, "Ultrafast all-optical differentiator," *Opt. Express*, vol. 14, no. 12, pp. 10699–10707, Oct. 2006.
- [8] Y. Park, J. Azaña, and R. Slavik, "Ultrafast all-optical first- and higher-order differentiators based on interferometers," *Opt. Lett.*, vol. 32, no. 6, pp. 710–712, Mar. 2007.
- [9] N. K. Berger, B. Levit, B. Fischer, M. Kulishov, D. V. Plant, and J. Azaña, "Temporal differentiation of optical signals using a phase-shifted fiber Bragg grating," *Opt. Express*, vol. 15, no. 2, pp. 371–381, Jan. 2007.
- [10] Y. Hu, *et al.*, "An ultra-high-speed photonic temporal differentiator using cascade SOI microring resonators," *J. Opt.*, vol. 14, no. 6, pp. 065501–065508, May 2012.
- [11] G. Zhou, *et al.*, "All-optical temporal differentiation of ultra-high-speed picosecond pulses based on compact silicon microring resonator," *Electron. Lett.*, vol. 47, no. 14, pp. 814–816, Jul. 2011.
- [12] F. Liu, *et al.*, "Compact optical temporal differentiator based on silicon microring resonator," *Opt. Express*, vol. 16, no. 20, pp. 15880–15886, Sep. 2008.
- [13] C. Cuadrado-Laborde and M. V. Andrés, "In-fiber all-optical fractional differentiator," *Opt. Lett.*, vol. 34, no. 6, pp. 833–835, Mar. 2009.
- [14] H. Shahoei, J. Albert, and J. P. Yao, "Optically tunable fractional order temporal differentiator using an optically pumped tilted fiber Bragg grating," *IEEE Photon. Technol. Lett.*, vol. 24, no. 9, pp. 370–372, May 1, 2012.
- [15] A. Yariv, "Universal relations for coupling of optical power between microresonators and dielectric waveguides," *Electron. Lett.*, vol. 36, no. 4, pp. 321–322, Feb. 2000.
- [16] D.-X. Xu, S. Janz, and P. Cheben, "Design of polarization-insensitive ring resonators in silicon-on-insulator using MMI couplers and cladding stress engineering," *IEEE Photon. Technol. Lett.*, vol. 18, no. 2, pp. 343–345, Jan. 15, 2006.
- [17] A. V. Oppenheim and J. S. Lim, "The importance of phase in signals," *Proc. IEEE*, vol. 69, no. 5, pp. 529–541, May 1981.